IIETA International Information and Engineering Technology Association
Advancing the World of Information and Engineering

Environmental and Earth Sciences Research Journal
Vol. 9, No. 3, September, 2022, pp. 104-113
Journal homepage: http://iieta.org/journals/eesrj

Petrographic and Kinematic Analysis of the Itombwe Synclinorium Formations Exposed at Tshondo and Bugoy (South-Kivu region, Democratic Republic of the Congo)

Aganze B. Gloire[1,2*], Masirika M. Lucien[1], Ganza B. Gloire[1], Nandezo W. Robert[1]

[1] Department of Geology, Université Officielle de Bukavu, Bukavu, P.O. Box 570, DRC
[2] Department of Physics and Earth Sciences, Jacobs University Bremen, Bremen, P.O. Box 28759, Germany

Corresponding Author Email: a.baciyunjuze@jacobs-university.de

https://doi.org/10.18280/eesrj.090304

Received: 2 July 2022
Accepted: 1 August 2022

Keywords:
Pan-African orogeny, metasedimentary rocks, mineral paragenesis, deformation phases, paleostress, DRC

ABSTRACT

The purpose of this study is to investigate the Itombwe synclinorium formations that were affected by the late Pan-African orogenesis in the nordeastern Congo. A variety of controversies surround Tshondo and Bugoy's tectonic evolution and associated metasedimentary formations. A field-based approach combined with paleostress inversion techniques and petrographic analyses were conducted on 190 structural measurements and 6 rock samples used in this study. The results reveal the presence of four major petrographic facies: conglomeratic facies (conglomerate and diamictite), carbonate facies (travertine), greenschist facies (graphitic black shale and pelite), as well as quatzitic facies (quartzite and sandstone). The mineral assemblages consisting of high contents (>70%) of muscovite/sericite and biotite albite, plagioclase, quartz, and some opaque minerals. With the assistance of Win-Tensor software, the kinematic analysis reveals two major deformation phases, (1) a ductile deformation phase (D1-2), which is associated with isoclinal folds and strike-slip faults, and (2) a submeridian brittle deformation phase (D2), which generated extensive faults trending NNW-SSE to NE-SW directions, while reactivating bedding surfaces (NE-SW) in a series of secondary faults. The findings of this research may assist geologists in conducting core logging operations and provide a baseline for understanding the relationship between rock, minerlization, and tectonics in mineral-rich areas.

1. INTRODUCTION

The Itombwe synclinorium, often referred to as the Neoproterozoic belt, is one of the geological units in Kivu region [1]. This elongated folded structure lies within the range of Lake Kivu between its northern shore and the nord-western shore of Lake Tanganyika [2]. In the upper Kibaran, it consists of two lithological units: lower and upper Kadubu, which are separated by faults [3, 4]. The rock formations outcropping in these two units have been mapped in differnt places, including Tshondo, Bugoy, Nya-Kaziba, Kigogo, Kalama, and Madubwe. Tshondo and Bugoy belong to the upper Kadubu unit, which contains rocks of varying sizes including sandstone, conglomerates, granites, gneisses and schists [5]. These conglomerates, reminiscent of glacial deposits, are called mixitites or diamicites [6, 7].

The Itombwe synclinorium, dated between 1020 ± 50 and 575 ± 83 Ma abounds with a plethora of mineralization, the most important of which is gold and some rare metals (Figure 2). They derivve from an albitite dyke (970 Ma) in the Kasika granite [8, 9].

Recent Pan-African tectonic events have severely strained this belt [3, 10]. However, other deformation phases are still debated today. Additionally, the growing interest in Tshondo and Bugoy's economic potential also calls for a more detailed petrographic study, which is a source to a wealth of information during core logging in mineral exploration.

The interpretations of kinematic indicators within a paraconglomerate by Walemba et al. [6, 8], revealed a jusxtaposition of two crustal blocks associated with E-W compressive stresses,as well as large-scale dextral/sinistral shearing but, the exact kinematic reationship between these faulting system at tshondo and bugoy is still unclear.

Similary, Lefevère [4] used remote sensing data and image interpretations to understand the deformation in the two areas inverstigated. He noted the presence of concemtric lineaments that he interpreted as resulting from 2 compression systems, associated with lithology such as shales, sandstones, quartizites and conglomerates. However, a detailed in-situ survey is always crucial to confirm what may at times not be captured remotely. In recent years, not much has been updated in terms of knowledge. Among the reasons are the difficulty of field access, active rugged terrains, and the risk of slope failure, among others.

Thus, the results highlighted in this paper provide an update and complete the general petrographic and structural knowledge available in the Neoproterozoic belt of South-Kivu, while shedding new light the stress regimes and petrographic types in these areas using modern techniques.

The study areas are located the eastern part of the Democratic Republic of the Congo and cover a total area of ca. 4 km^2. They are respectively bounded by longitudes 28.60°E and 28.75°E and latitudes -2.86°S and -2.92°S (Figure 1).

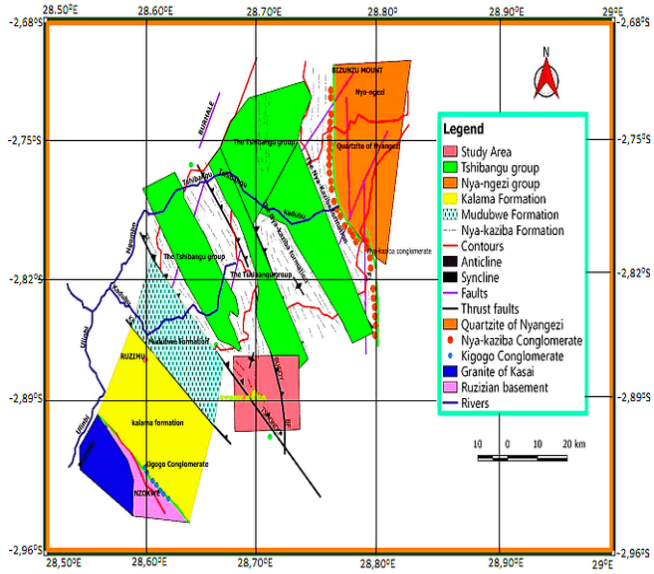

Figure 1. Location of the study areas and geology of the Itombwe synclinorium with its associated lithological units (modified from Villeneuve 1987)

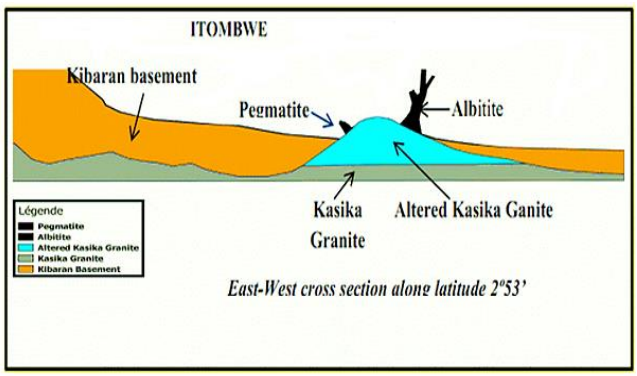

Figure 2. The origin of mineral deposits in the Itombwe Synclinorium [2]

2. METHODS

Over the course of one month, the two areas were mapped. Outcrop profiles were described on a macroscale. For each sampling station, the geographical coordinates were recorded. Fresh rock samples were collected, packed, and labelled for ex-situ analyses. A "Breithaupt-Kassel" compass was used to map linear and planar structures in the field. To make the interpretation of the data easier, the orientations were recorded in Dip/Dip direction format, then converted to Strike/Dip format. Thin-section microscopy was performed on 6 rock samples at the Geological Museum of Bukavu and optical observations were conducted at the Official University of Bukavu's mineralogical laboratory in plane-polarized and crossed-polarized light. FIJI (ImageJ) point counting software was used to calculate the mineral content of samples.

Structural measurements were computed using paleo stress inversion techniques in Win-tensor software 5.9.3, developed by Delvaux and Sperner [11], of which two methods are recognized: the classical R-Dihedron methods and the modern iterative Rotational Optimization Method [12, 13].

3. RESULTS AND DISCUSSION

3.1 Petrographic analysis

Rock samples were described macroscopically based on factors such as mineralogical composition, color, structure, weathering rate, and behavior after being exposed to hydrochloric acid. In contrast, microscopic descriptions of minerals were based on characteristics like color, pleochroism, habit, cleavage, relief, and twining [14].

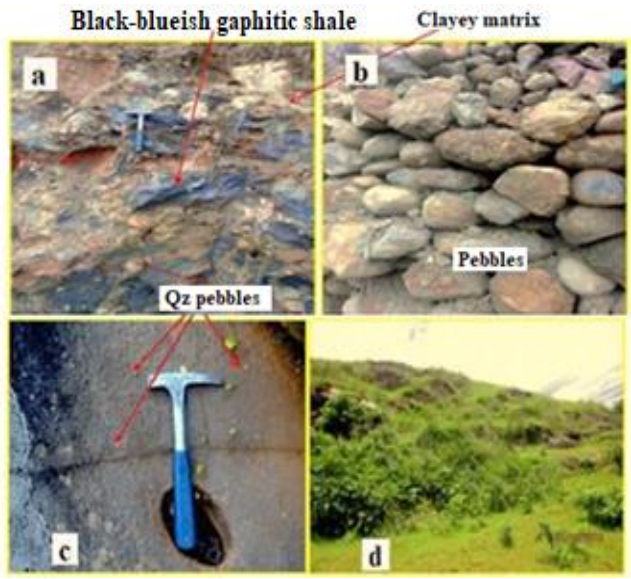

Figure 3. Conglomerate outcrop (a) and associated pebbles (b), used as retaining walls in the Rugenge mining quarry. Diamictite outcrop, also known as " paraconglomerate" (c). They are mostly found on the western slope of the Irongero River at Bugoy (d) and are believed to have been deposited during the latest Cryogenian glaciation (720-635 Ma)

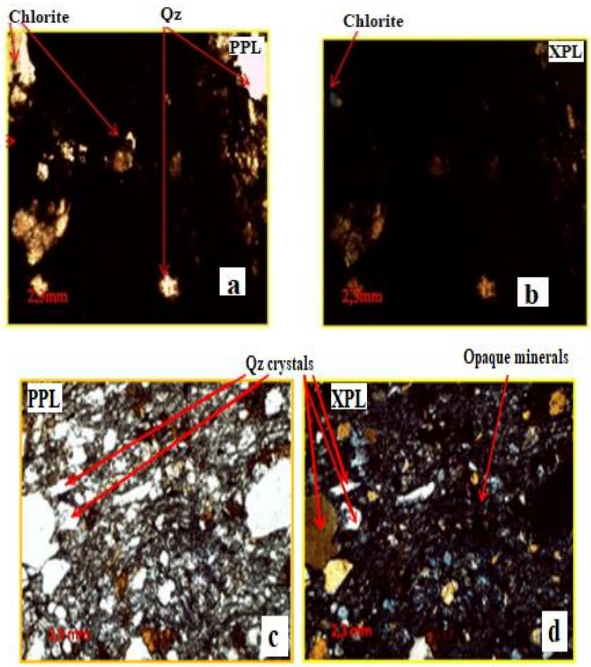

Figure 4. Microphotographs of conglomerate and diamictite: microscopic observations in plane polarized light (a, c) and crossed polarized light (b, d). Both rocks show large content in quartz crystals and opaque minerals

3.1.1 Rocks with conglomerate facies

Conglomerate and diamictite. Both sides of the Kadubu and Kashwa rivers are covered in Congolomerates. It consists of colorless mono-crystalline quartz grains (50-60%) along with medium relief chlorite (Figure 4a), which polarizes into yellowish gray and bluish green (Figure 4b) in a brown--reddish to yellowish ferruginous, clayey matrix Also present in the rock are fragments of polygenic and heterometric rocks consisting of black-blueish graphitic shales, rounded pebbles, sandstones, quartzites, and pelites measured in centimeters (Figure 3a), rounded pebbles, sandstones, quartzites, and pelites mostly in the order of centimeters (Figure 3b).

On the western slope of the Irongero River, a few miles north of Bugoy, diamictite outcrops were found (Figure 3c, d). A gray or black color characterizes them, and they are compact in nature. Quartz veins, granite, sandstone, gneiss, and quartzite clasts range in size from 1 to 15 cm long. They are strongly foliated in N-S directions and embedded in a chloritic clay matrix (Figure 4c, d).

3.1.2 Rocks with carbonate facies

Travertine. This rock was sampled from the Karhendezi-Bugoy geothermal field. In essence, it is a calcareous concretion with a rough surface (massive structure). The soil is predominantly clayey-graphite with veins of quartz (1 cm thick), rich in red iron oxides and calcite. A dozen hot springs are located on either side of the Karhendezi-Cidubwe river (Figure 5a, b). Several dissolved minerals, including sulfur, contribute to a rotten egg-like smell in the water, which is between 65°C and 73°C.

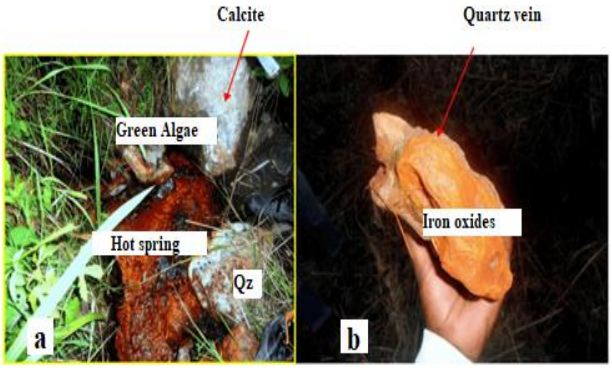

Figure 5. A travertine deposit surrounded by green algae at the emergence of a geothermal spring(a). Sample of travertine (b)

3.1.3 Rocks with greenschist facies

Pelite and graphitic black shale These are clayey rocks that have been indurated and stratified by compaction. Throughout the study area, they are found in black-grayish and yellowish colors. (Figure 6a, b) shows pelite cleavages that are slightly fresh on matte surfaces. A microscopic examination of the rock shows quartz (20-40%), sericite (15-20%), and chlorite (10-15%); there is a second order birefringence and the rock is polarizing into a greenish color with a right extinction angle (Figure 7a, b). Graphitic black shale, like pelite, exhibits a flaky texture due to foliation (Figure 6c, d) containing quartz crystals (15%), recrystallized pyrite (50%), carbon (10%), and muscovite (5%) (Figure 7c, d).

Figure 6. A pelite outcrop from Bugoy area (a) and a corresponding sample (b). Outcrop of graphitic schists from Tshondo (c) and eroded sample (d) collected along Musheke river valley

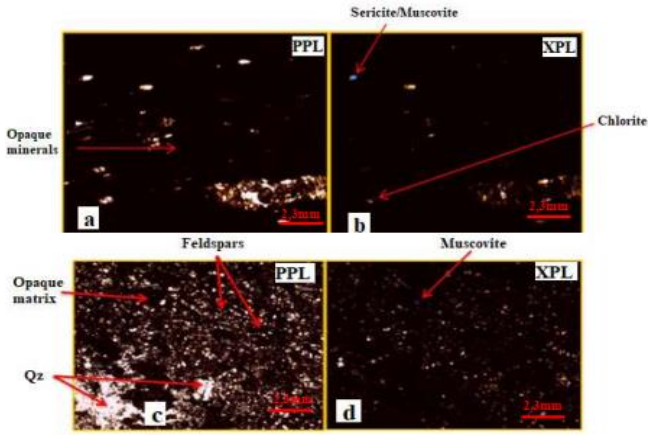

Figure 7. Microphotographs of pelite and graphitic schist (shale): microscopic observations in plane polarized light (a, c) and crossed polarized light (b, d)

3.1.4 Rocks with quartzitic facies

Quartzites. Their mineral composition consists of quartz minerals along with hematite, muscovite, biotite, and K-feldspar. Those found at Tshondo exhibit a superficial alteration of the type "cargneule-type" which is characterized by decayed and vacuolar habits (Figure 8). Quartz crystals appear as transparent patches under a microscope, whereas metallic minerals appear opaque. There are irregular shapes and xenomorphic properties to these minerals. Small elongated prisms of alkaline feldspar are also colorless. With relatively high relief and dark brown to greenish pleochroism, the yellow-browned absorption minerals represent biotite. Cross-polarized light shows bright polarization colors ranging from gray to white with an undulatory extinction, indicating a positive deformation, but difficult to detect. An elongated and attenuated polarization tint is present in biotite. Due to the mass of opaque minerals, orthoclase shows an oblique extinction and Carlsbad twinning associated with two crystals (Figure 9a, b).

Auriferous quartzite, which is composed primarily of metallic minerals (here Au), is also analyzed. Gaseous

inclusions appear as small bubbles. The colorlessness of mucovite can be attributed to its pleochroism, ranging from yellow to pale yellow (Figure 9c, d).

Figure 8. Sample of a Cargneule Quartzite from Tshondo

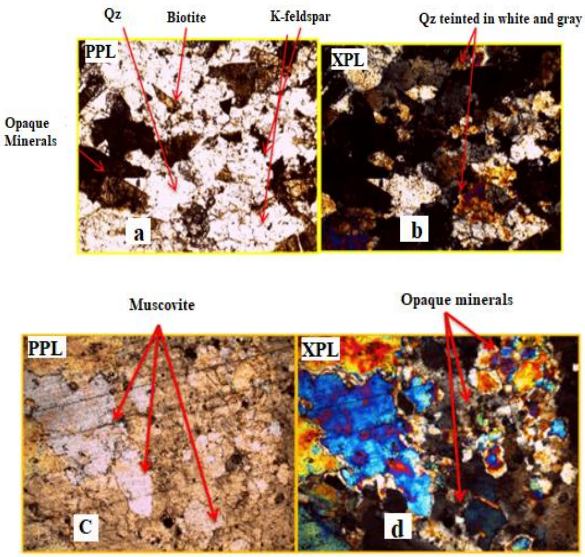

Figure 9. Microphotograph of ferriferous quartzite and gold-bearing quartz: in plane polarized light (a, c) and crossed polarized light (b, d)

3.2 Kinematic analysis

A total of 190 linear and planer features were analyzed. Subset indexes were used for conjugates shear fractures, fracture planes, extensive fractures, joints as well as foliation and bedding surfaces (Appendix Table 1, Table 2, and Table 3). In both areas, these measurements were used to quantify deformation.

Only a few faults with sense of movement were recorded due to the physical properties of the rock formations at Tshondo and Bugoy (friable, unconsolidated graphitic schists). It was not possible to collect a lot of data since fault planes are sparsely carved with tectoglyphs (Figure 10). In our opinion, erosion or other exogenous factors could have crumbled and erased most of the markers. A total of thirteen striae were correctly identified. As a result of their poor pronunciation, others were considered "Probable" and overlooked during the analysis process. The Striae have a preferential trend towards the NE-SW and NNE-SSW directions. There are two structural preferential trends for he fractures, bedding planes, and foliation: NE-SW and NNE-SSW (Figure 11a, b).

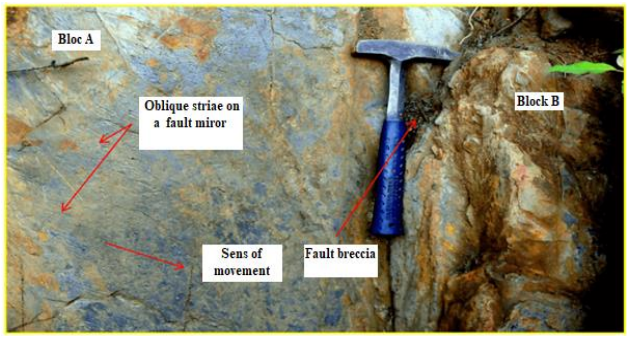

Figure 10. Striae appearing on a fault mirror and fault breccia made up with a mixture of clays and pellitic rocks

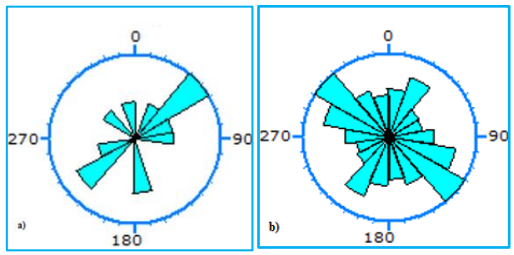

Figure 11. Rose diagram showing average statistical orientations for linear (a) and planar (b) measurements

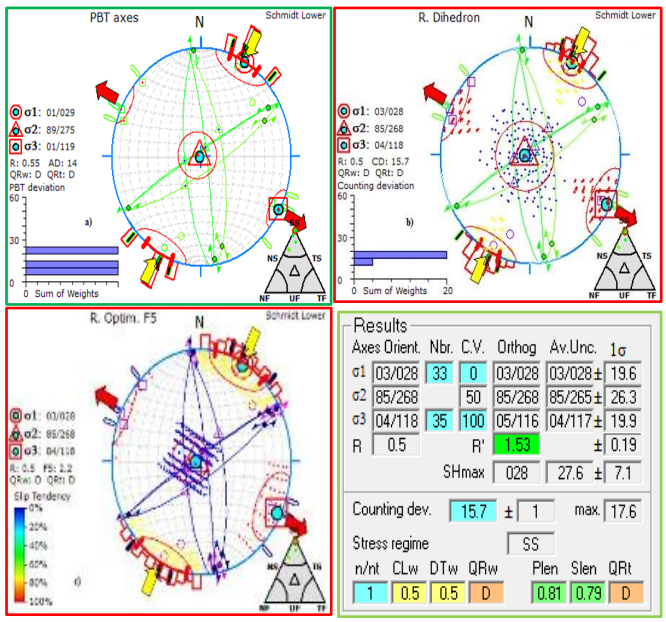

Figure 12. Stereoplots after optimization and separation: from PBT axes, R.Dihedron and R.Optim Methods(a, b, c) and final results for stress parameters (Reduced stress tensor, orientation of the horizontal principal stress axes and the stress regime

In accordance with Anderson's theory (Figure 14), kinematic analysis using Win-tensor software indicates two phases of deformation, highlighted by a strike-slip stress regime such that σ_1: N118º/03º SE, σ_2: N358º/85º SE, σ_3:N 208º/04º SW ($\sigma_2 \geq \sigma_3 \geq \sigma_1$) and an average stress ratio index R'=1.53 (Figure 12a, b, c), as well as a an pure extensive regime with stress ratio R= 0.46 (Figure 13). The principal stress axes are such that σ_1: N90º/65ºS, σ_2: N186º/23ºSE, σ_3:N250º/9ºSW ($\sigma_1 \geq \sigma_2 \geq \sigma_3$). The values were obtained following subsequent tensor optimization and data separation based on Dihedron methods, which requires the background

minimum counting deviation value (C.V) representing σ_1 in the counting grid to be equal to 0 and the maximum counting deviation value representing σ_3 to be equal to 100 [11].

As shown by Villeneuve et al. [3, 6, 8, 15] and other reseachers who have investigated the Itombwe Synclinorium, Tshondo and Bugoy, as we have also just seen, have undergone a small-scale regional metamorphism, evolving towards greenschist facies and an important granitization highlighted by the Kasika granitic intrusion, but geochronological studies are needed.

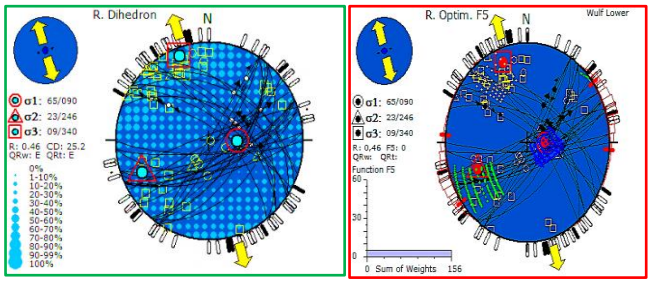

Figure 13. Stereoplots after optimization and separation for conjugated fractures and faults without senses of movement: R.Dihedron and R.Optim Methods (a, b)

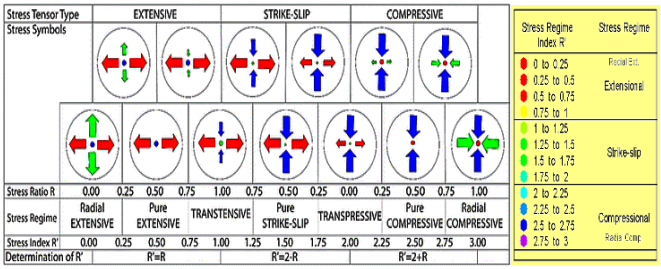

Figure 14. Stress regime and stress tensor types according to Anderson deformation theory [11]

Microscopic analyses of thin sections of rocks as well as different macroscopic observations have shown a mineral paragenesis mainly made of chlorites, muscovites / sericites and biotites, and metallic minerals. Observations also revealed large ranges of quartz which recrystallized under mono and polycrystalline crystals presenting undulatory to right extinctions.

Admittedly, traces of deformation were not detectable. It is believed that long after their formation, these lithological units underwent an orogeny marked by strong fracturing and a slightly to more pronounced crushing following N-S directions. Foliation is the most dominant structural feature and the most penetrating at the scale of the outcrops. This foliation probably corresponds to the major deformation phase in the Itombwe. It is associated with local folds testified by the Kinematic analysis performed on faults with movement. However, a second deformation is evidenced.

4. CONCLUSION

Investigations at Tshondo and Bugoy reveals four petrography facies mainly made of rocks such as graphitic schist, pelite, conglomerate, paraconglomerate, travertines, quartzites, and sandstone.They have undergone a strong to weak metamorphism that has evolved in the facies of green schists with quartz, chlorite, muscovite, biotite, and opaque minerals as dominant mineral assemblages.

The estimation of stress tensors using inversion techniques by Anderson [16] reveals pure strike-slip and extensive deformation phases. This is tangible proof that at least two phases of deformation have occurred in the geological formations outcropping at Tshondo and Bugoy. First, a ductile deformation phase D1-2 which generated isoclinal folds and then a submeridian brittle deformation which generated thrusting faults of Tshondo and Bugoy while reactivating stratification surfaces in a series of secondary faults trending NE-SW.

In order to complete this study, the following must be done in the future:

- Conduct a non-hasty lithostratigraphic study at Tshondo and Bugoy by drilling deep to determine the thickness of related formations.
- Polish sections of rocks in order to combine the mineral parageneses of greenschist facies with the parageneses of metallic minerals (opaque minerals).
- Analyze and characterize the faults affecting the formations in both areas, relying not on structural markers, but instead on morphological markers in direct field observation.
- Date both areas' geological formations geochronologically and compare their ages with the ages established in the itombwe.

ACKNOWLEDGMENT

The authors acknowledge the help and support provided by the Department of Geology of the Official University of Bukavu. The authors declare that no funds, grants, or other support were received during the preparation of this manuscript.

REFERENCES

[1] Lepersonne, J. (1971). Les formations du soubassement au Maniema et au Kivu. Belgium, Tervuren.

[2] Villeneuve, M. (1978). Etude Photogéologique du Secteur Precambrien de Luemba (Sud-Kivu-Zaire) la partie Meridionale du "Synclinal de L'itombwe" et son Substratum. Annales de La Société Géologique de Belgique, 101: 47-52. https://popups.uliege.be/0037-9395/index.php?id=4379.

[3] Villeneuve, M. (1987). Géologie du Synclinal de l'Itombwe (Zaire Oriental) et le Problème de l'existence d'un Sillon Plissé Pan-Africain. Journal of African Earth Sciences, 9(6): 869-880. https://doi.org/10.1016/0899-5362(87)90046-7

[4] Lefevère, J. (2003). Analyse et interprétation des canevas lithostratigraphiques et tectoniques du Synclinal de l'Itombwe (Sud-Kivu République Démocratique du Congo) à l'aide des données satellitaires et radar. Université Libre de Buxelles.

[5] Lhoest, A. (1946). Une coupe remarquable des couches de base de l'Urundi, dans l'Itombwe (Congo belge). Annales de La Société Géologique de Belgique., 69(B): 250-256.

[6] Walemba, K.M. (2001). Geology, geochemistry, and tectono-metallogenic evolution of Neoproterozoic gold

deposits in the Kadubu area, University of the Witwatersrand. http://hdl.handle.net/10539/15209, accessed on June 17, 2022.
[7] Peeters, L. (1952). Observations géomorphologiques et géologiques au Sud-Ouest de Costermansville (Kivu). Annales Du Musée Du Congo Belge, 8(10): 9-62. http://bibliotheque.donboscordc.org/index.php?lvl=notice_display&id=1331.
[8] Walemba, K.M.A., Master, S. (2005). Neoproterozoic diamictites from the Itombwe Synclinorium, Kivu Province, Democratic Republic of Congo: Palaeoclimatic significance and regional correlations. Journal of African Earth Sciences, 42(1-5): 200-210. https://doi.org/10.1016/j.jafrearsci.2005.08.009
[9] Villeneuve, M., Chorowicz, J. (2004). Les sillons plissés du Burundien supérieur dans la chaine Kibarienne d'Afrique centrale. Geosciences, 336(9): 807-814. https://doi.org/10.1016/j.crte.2004.01.006
[10] Villeneuve, M. (1977). Précambrien du Sud du lac Kivu. Etude stratigraphique, pétrographique et tectonique, Fac. Sci et Techn. St Jérôme, 1977. https://doi.org/10.2113/gssgfbull.S7-XX.6.915
[11] Delvaux, D., Sperner, B. (2003). New aspects of tectonic stress inversion with reference to the TENSOR program. The Geological Society of London, 212: 75-100. http://dx.doi.org/10.1144/GSL.SP.2003.212.01.06
[12] Angelier, J. (1994). Fault slip analysis and paleostress reconstruction. Continental Deformation, 4: 101-120.
[13] Angelier, J., Tarantola, A., Manoussis, S. (1982). Inversion of field data in fault tectonics to obtain the regional stress — I. Single phase fault populations: A new method of computing the stress tensor. Geophysical Journal of the Royal Astronomical Society, 69(3): 607-621. https://doi.org/10.1111/j.1365-246X.1982.tb02766.x
[14] Hutchinson, C. (1974). Laboratoty Handbook of Petrographic Techniques. Wiley, New York. https://doi.org/10.1017/S001675680004574X
[15] Rumvegeri, B. (1987). Le Précambrien de l'Ouest du lac Kivu et sa place dans l'évolution géodynamique de l'Afrique centrale et oriental: pétrologie et Tectonique, St Jérôme.
[16] Anderson, E.M. (1905). The dynamics of faulting. Transactions of the Edinburgh Geological Society, 8(3): 387-402. https://doi.org/10.1144/transed.8.3.387

NOMENCLATURE

Cm	Centimetres
C.V	Counting deviation value
D1	Deformation 1
D2	Deformation 2
DRC	Democratic Republic of the Congo
km	Kilometres
Ma	Million years
PBT	Pressure tension and null axis
PPL	Plane Polarized Light
XPL	Crossed-Polarized Light
σ_1	Principal stress axis sigma 1
°C	Celcius degree

APPENDICES

Table 1. Structural measurements for striation and analytical results

Striae						
ID	Lat (degree)	Long X (degree)	Alt Z (m)	Plane	Line	Sense
1	-2,87464	28,65513	1310	62/052	33/342	NS
2	-2,87731	28,65761	1311	79/029	26/305	NS
3	-2,87731	28,65761	1310	79/029	43/310	NS
4	-2,87731	28,65761	1454	44/026	44/028	IS
5	-2,87731	28,65761	1454	40/034	38/057	IS
6	-2,87731	28,65761	1454	40/027	38/050	IS
7	-2,8746	28,65511	1314	81/231	59/156	NS
8	-2,8746	28.65511	1314	30/305	05/223	NS
9	-2,87435	28,65801	1373	64/045	62/068	IS
10	-2,87435	28,65801	1373	64/045	63/057	IS
11	-2,87435	28,65801	1373	64/045	53/095	IS
12	-2,87435	28,65801	1373	40/088	39/071	NS
13	-2,87435	28,65801	1373	64/045	64/049	IS

Table 1. Continued

Kinematic Axes						Stress Parameters		
PIncl	P Azim	B Incl	B Azim	T Incl	T Azim	Shmax	Shmin	R'
46	285	44	111	3	18	107	17	1
26	254	61	98	10	349	77	167	1.5
38	249	45	108	20	356	79	169	1
1	207	1	297	89	72	27	117	2.5
6	227	11	318	77	109	46	136	2.5
6	220	11	311	77	102	39	129	2.5
46	81	29	316	30	207	104	14	1
42	195	30	316	34	68	174	84	1
18	53	9	320	69	204	57	147	2.5
19	49	5	317	71	213	51	141	2.5

15	65	24	328	61	183	70	160	2.5
81	22	8	168	6	259	170	80	0.5
46	2	316	71	221	47	137	2.5	2

Table 2. Structural measurements for conjugated fractures and analytical results

Conjugated Fractures					
ID	Lat (degree)	Long (degree)	Alt (m)	Fracture 1(degree)	Fracture 2(degree)
1	-2.87731	28.65761	1365	85/330	14/059
2	-2.87541	28.65461	1340	75/265	02/355
3	-2.87464	28.65514	1310	89/302	26/032
4	-2.87464	28.65514	1310	78/150	23/065
5	-2.87474	28.6551	1314	70/080	16/164
6	-2.79596	28.68737	1520	84/320	25/233
7	-2.79829	28.68514	1521	85/082	06/171
8	-2.79829	28.68514	1521	86/330	07/240
9	-2.79829	28.68514	1521	75/135	18/220
10	-2.79829	28.68514	1521	86/164	23/252

Table 2. Continued

	Kinematic Axes					**Stress Parameters**		
PIncl	P Azim	B Incl	B Azim	T Incl	T Azim	Shmax	Shmin	R'
26	9	75	259	12	118	27	117	1.5
26	9	75	259	12	118	27	117	1.5
49	25	64	214	6	316	47	137	1.5
49	25	64	214	6	316	47	137	1.5
197	25	64	38	8	291	19	109	1.5
197	25	64	38	8	291	19	109	1.5
206	8	82	30	1	296	26	116	1.5
206	8	82	30	1	296	26	116	1.5
236	21	67	83	10	330	58	148	1.5
236	21	67	83	10	330	58	148	1.5

Table 3. Structural measurements for bedding planes, fractures plane, joints, and foliation

Bedding planes, fracture planes, joints, foliation					
ID	Lat Y (degree)	Long X (degree)	Alt Z (m)	Dip-angle/Dip-direction (degree)	Type
1	-2.87464	28.65514	1522	85/320	Fracture plane
2	-2.87464	28.65514	1522	85/305	Fracture plane
3	-2.87474	28.6551	1522	85/150	Fracture plane
4	-2.87474	28.6551	1522	63/104	Fracture plane
5	-2.87515	28.65637	1705	80/175	Fracture plane
6	-2.87515	28.65637	1705	37/350	Fracture plane
7	-2.87562	28.65441	1721	75/300	Fracture plane
8	-2.87515	28.65637	1721	72/175	Fracture plane
9	-2.87515	28.65637	1721	37/175	Fracture plane
10	-2.87731	28.65761	1721	80/122	Fracture plane
11	-2.87731	28.65761	1721	80/122	Fracture plane
12	-2.87731	28.65761	1721	85/076	Fracture plane
13	-2.87688	28.65811	1721	79/042	Fracture plane
14	-2.87688	28.65811	1688	75/043	Fracture plane
15	-2.87688	28.65811	1688	76/040	Fracture plane
16	-2.87688	28.65811	1688	70/042	Fracture plane
17	-2.87688	28.65811	1688	75/040	Fracture plane
18	-2.87818	28.65897	1688	75/044	Fracture plane
19	-2.87691	28.65874	1672	76/045	Fracture plane
20	-2.87688	28.65811	1672	89/052	Fracture plane
21	-2.87688	28.65811	1672	87/055	Fracture plane
22	-2.87923	28.66048	1672	74/110	Fracture plane
23	-2.87691	28.65874	1672	66/091	Fracture plane
24	-2.87691	28.65874	1654	86/336	Fracture plane
25	-2.87691	28.65874	1654	88/352	Fracture plane
26	-2.87691	28.65874	1654	65/263	Fracture plane
27	-2.87691	28.65874	1654	49/037	Fracture plane
28	-2,87562	28,65441	1355	20/099	Bedding plane
29	-2,87491	28,65592	1348	61/255	Bedding plane

30	-2,87491	28,65592	1348	61/262	Bedding plane
31	-2,87515	28,65637	1365	86/262	Bedding plane
32	-2,87515	28,65637	1365	85/092	Bedding plane
33	-2,87515	28,65637	1365	85/272	Bedding plane
34	-2,87515	28,65637	1365	80/264	Bedding plane
35	-2,87515	28,65637	1365	80/272	Bedding plane
36	-2,87731	28,65761	1454	84/272	Bedding plane
37	-2,87731	28,65761	1454	85/122	Bedding plane
38	-2,87731	28,65761	1454	71/122	Bedding plane
39	-2,87731	28,65761	1454	76/142	Bedding plane
40	-2,87731	28,65761	1454	80/150	Bedding plane
41	-2,87688	28,65811	1416	85/110	Bedding plane
41	-2,87688	28,65811	1416	85/010	Bedding plane
42	-2,87688	28,65811	1416	16/185	Bedding plane
43	-2,87688	28,65811	1416	42/089	Bedding plane
44	-2,87818	28,65897	1409	75/022	Bedding plane
45	-2,87818	28,65897	1409	10/002	Bedding plane
46	-2,87691	28,65874	1356	65/008	Bedding plane
47	-2,87691	28,65874	1356	40/290	Bedding plane
48	-2,87691	28,65874	1356	60/282	Bedding plane
49	-2,87691	28,65874	1356	50/280	Bedding plane
50	-2,87691	28,65874	1356	70/120	Bedding plane
51	-2,87691	28,65874	1356	80/274	Bedding plane
52	-2,87691	28,65874	1356	79/007	Bedding plane
53	-2,87691	28,65874	1356	20/228	Bedding plane
54	-2,87691	28,65874	1356	71/112	Bedding plane
55	-2,85733	28,65827	1345	74/110	Bedding plane
56	-2,85733	28,65827	1345	66/091	Bedding plane
57	-2,85733	28,65827	1345	86/336	Bedding plane
58	-2,85733	28,65827	1345	88/352	Bedding plane
59	-2,85733	28,65827	1345	65/263	Bedding plane
60	-2,87568	28,65882	1380	49/037	Bedding plane
61	-2,87568	28,65882	1380	20/099	Bedding plane
62	-2,87584	28,65888	1363	85/350	Bedding plane
63	-2,87584	28,65888	1363	81/002	Bedding plane
64	-2,87584	28,65888	1363	81/012	Bedding plane
65	-2,8741	28,65462	1319	85/144	Bedding plane
66	-2,8741	28,65462	1319	87/030	Bedding plane
67	-2,87397	28,65886	1318	87/184	Bedding plane
68	-2,87458	28,65505	1315	75/218	Bedding plane
69	-2,8746	28,65511	1314	85/023	Bedding plane
70	-2,85509	28,656	1352	75/046	Bedding plane
71	-2,85509	28,656	1352	87/200	Bedding plane
72	-2,87542	28,67637	1381	80/198	Bedding plane
73	-2,87542	28,67637	1381	89/024	Bedding plane
74	-2,87841	28,65871	1456	71/210	Bedding plane
75	- 2,87904	28,66027	1511	88/190	Bedding plane
76	-2,87812	28,659	1420	80/190	Bedding plane
77	-2,87812	28,659	1420	80/144	Bedding plane
78	-2,87549	28,65672	1392	81/200	Bedding plane
79	-2,87549	28,65672	1392	76/200	Bedding plane
80	-2,87472	28,65511	1318	84/032	Bedding plane
81	-2,87476	28,65503	1317	89/032	Bedding plane
82	-2,87435	28,65801	1373	85/222	Bedding plane
83	-2,87167	28,6783	1398	80/010	Bedding plane
84	-2,87167	28,6783	1398	82/200	Bedding plane
85	-2,87167	28,6783	1398	89/190	Bedding plane
86	-2,87546	28,65895	1330	85/182	Bedding plane
87	-2,87564	28,65927	1346	89/006	Bedding plane
88	-2,87482	28,65847	1316	75/042	Bedding plane
89	-2.87443	28.65554	1311	85/045	Foliation
90	-2.87208	28.67290	1409	71/042	Foliation
91	-2.87208	28.67290	1409	70/044	Foliation
92	-2.87208	28.67290	1409	88/034	Foliation
93	-2.87208	28.67290	1409	85/032	Foliation
94	-2.87443	28.65554	1311	74/035	Foliation
95	-2.782	28.68537	1512	71/032	Foliation
96	-2.782	28.68537	1512	85/044	Foliation

97	-2.782	28.68537	1512	75/052	Foliation
98	-2.782	28.68537	1512	52/032	Foliation
99	-2.782	28.68537	1512	67/054	Foliation
100	-2.782	28.68537	1512	66/050	Foliation
101	-2.79817	28.68407	1522	45/044	Foliation
102	-2.79817	28.68407	1522	70/060	Foliation
103	-2.79817	28.68407	1522	49/022	Foliation
104	-2.87464	28.65514	1310	53/034	Fracture plane
105	-2.87464	28.65514	1310	65/052	Fracture plane
106	-2.87474	28.6551	1314	61/055	Fracture plane
107	-2.87474	28.6551	1314	39/032	Fracture plane
108	-2.87515	28.65637	1365	75/063	Fracture plane
109	-2.87515	28.65637	1365	45/042	Fracture plane
110	-2.87562	28.65441	1355	45/052	Fracture plane
111	-2.87515	28.65637	1365	41/044	Fracture plane
112	-2.87515	28.65637	1365	40/041	Fracture plane
113	-2.87731	28.65761	1454	39/032	Fracture plane
114	-2.87731	28.65761	1454	42/024	Fracture plane
115	-2.87731	28.65761	1454	44/058	Fracture plane
116	-2.87688	28.65811	1416	44/043	Fracture plane
117	-2.87688	28.65811	1416	53/030	Fracture plane
118	-2.87688	28.65811	1416	37/016	Fracture plane
119	-2.87688	28.65811	1416	44/044	Fracture plane
120	-2.87688	28.65811	1416	40/042	Fracture plane
121	-2.87818	28.65897	1409	42/045	Fracture plane
122	-2.87691	28.65874	1356	35/032	Fracture plane
123	-2.87688	28.65811	1416	39/034	Fracture plane
124	-2.87688	28.65811	1416	39/030	Fracture plane
125	-2.87923	28.66048	1551	64/069	Fracture plane
126	-2.87691	28.65874	1356	65/069	Fracture plane
127	-2.87691	28.65874	1356	49/026	Fracture plane
128	-2.87691	28.65874	1356	50/028	Fracture plane
129	-2.87691	28.65874	1356	41/022	Fracture plane
130	-2.87691	28.65874	1356	38/010	Fracture plane
131	-2.87691	28.65874	1356	44/140	Fracture plane
132	-2.87691	28.65874	1356	85/052	Fracture plane
133	-2.87691	28.65874	1356	72/042	Fracture plane
134	-2.87691	28.65874	1356	60/035	Fracture plane
135	-2.87568	28.65882	1380	59/020	Fracture plane
136	-2.87584	28.65888	1363	70/038	Fracture plane
137	-2.87584	28.65888	1363	64/044	Fracture plane
138	-2.87464	28.65514	1310	61/018	Fracture plane
139	-2.87585	28.65409	1368	54/038	Joint
140	-2.87620	28.67660	1440	68/035	Joint
141	-2.87701	28.65816	1414	70/028	Joint
142	-2.87868	28.66009	1492	66/048	Joint
143	-2.87496	28.65596	1349	67/052	Joint
144	-2.87196	28.673	1416	49/028	Joint
145	-2.87516	28.65844	1325	53/032	Joint
146	-2.79596	28.68737	1520	40/056	Joint
147	-2.79829	28.68514	1521	60/082	Joint
148	-2.79829	28.68514	1521	55/050	Joint
149	-2.79829	28.68514	1521	60/064	Joint
150	-2.79829	28.68514	1521	46/036	Joint
151	-2.79829	28.68514	1521	46/014	Joint
152	-2.79817	28.68407	1522	81/040	Joint
153	-2.79817	28.68407	1522	75/030	Joint
154	-2.79817	28.68407	1522	70/050	Joint
155	-2.79817	28.68407	1522	57/010	Joint
156	-2.8225	28.68217	1705	56/010	Joint
157	-2.82297	28.68180	1721	50/070	Joint
158	-2.82297	28.68180	1721	72/023	Joint
159	-2.82297	28.68180	1721	65/034	Joint
160	-2.82297	28.68180	1721	59/045	Joint
161	-2.82126	28.68261	1672	75/132	Joint
162	-2.83088	28.69354	1702	85/118	Joint
163	-2.83088	28.69354	1702	81/112	Joint
164	-2.83010	28.69312	1704	65/124	Joint

165	-2.83010	28.69312	1704	88/288	Joint
166	-2.79596	28.68737	1520	84/300	Joint